OmoMYC blunts promoter invasion by oncogenic MYC to inhibit gene expression characteristic of MYC-dependent tumors

Lisa Anna Jung[1,2,8], Anneli Gebhardt[1,8], Wolfgang Koelmel[2], Carsten Patrick Ade[1],

Susanne Walz[3], Jochen Kuper[2], Bjoern von Eyss[1], Sebastian Letschert[4], Cornelia Redel[1],

Luana d'Artista[5], Andrew Biankin[6], Lars Zender[5], Markus Sauer[4], Elmar Wolf[1], Gerard

Evan[7], Caroline Kisker[2,*], and Martin Eilers[1,*]

[1] Theodor Boveri Institute, Biocenter, University of Würzburg, Am Hubland, 97074 Würzburg, Germany

[2] Rudolf Virchow Center for Experimental Biomedicine, University of Würzburg, Josef-Schneider-Str. 2, 97080 Würzburg, Germany

[3] Comprehensive Cancer Center, Core Unit Bioinformatics, Biocenter, Am Hubland, 97074 Würzburg, Germany

[4] Department of Biotechnology and Biophysics, Biocenter, University of Würzburg, Am Hubland, 97074 Würzburg, Germany

[5] Division of Translational Gastrointestinal Oncology, Department of Internal Medicine I, University of Tübingen, 72076 Tübingen, Germany

[6] Wolfson Wohl Cancer Research Centre, Institute of Cancer Sciences, University of Glasgow, Garscube Estate, Switchback Road, Bearsden, Glasgow, Scotland G61 1BD, United Kingdom; West of Scotland Pancreatic Unit, Glasgow Royal Infirmary, Glasgow G31 2ER UK; South Western Sydney Clinical School, Faculty of Medicine, University of NSW, Liverpool NSW 2170, Australia

[7] Department of Biochemistry, University of Cambridge, 80 Tennis Court Road, Cambridge CB2 1GA, UK

[8] These authors contributed equally to the work.

[*] Correspondence: martin.eilers@biozentrum.uni-wuerzburg.de;caroline.kisker@virchow.uni-wuerzburg.de

Abstract

MYC genes have both essential roles during normal development and exert oncogenic functions during tumorigenesis. Expression of a dominant-negative allele of MYC termed OmoMYC can induce rapid tumor regression in mouse models with little toxicity for normal tissues. How OmoMYC discriminates between physiological and oncogenic functions of MYC is unclear. We have solved the crystal structure of OmoMYC and show that it forms a stable homodimer and as such recognizes DNA in the same manner as the MYC/MAX heterodimer. OmoMYC attenuates both MYC-dependent activation and repression by competing with MYC/MAX for binding to chromatin, effectively lowering MYC/MAX occupancy at its cognate binding sites. OmoMYC causes the largest decreases in promoter occupancy and changes in expression on genes that are invaded by oncogenic MYC levels. A signature of OmoMYC-regulated genes defines subgroups with high MYC levels in multiple tumor entities and identifies novel targets for the eradication of MYC-driven tumors. (149 words)

Key words: MYC, OmoMYC, promoter invasion, BOP1, ADRM1, ATAD3A

Introduction

A large body of evidence shows that the deregulated and enhanced expression of one of three members of the *MYC* gene family (*MYC*, *MYCN*, *MYCL*) contributes to the genesis of multiple human tumors[1]. MYC proteins are transcription factors that bind to virtually all promoters with an open chromatin structure as well as to thousands of enhancers together with an obligate heterodimerization partner, MAX (for recent reviews, see:[1-3]). They can both activate and repress genes transcribed by RNA polymerase II and, in some circumstances, enhance expression of all genes. In addition, MYC proteins can stimulate transcription of genes transcribed by RNA polymerases I and III.

Depletion of MYC in tissue culture or deletion of *MYC* or *MAX* genes during mouse development shows that MYC/MAX complexes have essential functions during embryonic development and are necessary for growth of multiple cell types *in vivo* and in culture[4-6]. This correlates with the observation that multiple target genes of MYC encode proteins involved in basic cellular processes, including protein translation, cell cycle progression, DNA synthesis and intermediary metabolism[1]. A plethora of mutations that initiate tumorigenesis leads to constitutive, growth factor-independent expression of MYC. During tumor progression, there is a strong selection for further increases in MYC expression to supra-physiological levels, suggesting that such high levels of MYC provide an additional advantage to tumor cells[7, 8]. Two models have been proposed to account for this selective pressure: in one, oncogenic levels of MYC acquire new functions not shown by physiological MYC such as effects on the tumor microenvironment[9], angiogenesis and response to hypoxia[10, 11], resistance to antimitogenic signals[12, 13], as well as stem cell function and metastasis[14]. In the second model, oncogenic MYC levels drive physiological processes such as translation to supra-physiological levels and tumor-specific phenotypes arise as stress responses to these primary events[15, 16].

The clearest demonstration that physiological and oncogenic functions of MYC can be discriminated comes from the study of a dominant-negative allele of MYC termed OmoMYC[17]. Mice expressing OmoMYC in a doxycycline-inducible manner display rapid

regression of lung adenocarcinomas, glioblastomas and pancreatic tumors but show only mild and fully reversible effects on proliferation in normal tissues[9, 17, 18]. As consequence, intermittent induction of OmoMYC ("metronomic treatment") enables long-term suppression of tumor growth arguing that therapeutic strategies that mimic OmoMYC may have significant efficacy for the treatment of human tumors[19].

OmoMYC comprises the carboxy-terminal basic region, helix-loop-helix and leucine zipper of MYC and carries four point mutations in the leucine zipper that are intended to alter its dimerization properties[20]. Here, we present an analysis of the OmoMYC structure, its genome-wide chromatin binding and gene regulation to understand its astounding ability to discriminate physiological from oncogenic functions of MYC.

Results

OmoMYC is a highly stable homodimer and forms a tight protein-DNA complex

To understand how OmoMYC regulates gene expression, we expressed a histidine-tagged OmoMYC protein in *E. coli* and purified the recombinant protein to homogeneity using sequential metal affinity and cation exchange chromatography (Supplementary Figure S1a,b). In parallel, we purified recombinant proteins encompassing the basic region/helix-loop-helix/leucine zipper (b/HLH/Zip) region of MYC and full length MAX (Supplementary Figure S1b). We pursued crystallization of OmoMYC in the absence and presence of an oligonucleotide carrying an E-box binding site and solved both the apo- and the DNA bound-structure of OmoMYC (Figure 1a,b; Supplementary Table S1a,b) at 1.95 Å and 2.70 Å, respectively. In both structures OmoMYC forms a homodimer with an overall structure that is very similar to those of other b/HLH/Zip structures, in particular to that of MYC/MAX heterodimers[21] (Supplementary Table S2a,b).

Superposition of the apo- and DNA-bound OmoMYC complex showed that the two structures are nearly identical with rms deviations of 0.60 Å for all main chain atoms with the exception of the basic region, which was not resolved in the apo-structure (Supplementary Table S2a). The homodimer is stabilized by multiple ionic and hydrophobic interactions (Figure 1c, Supplementary Figure S1c; Supplementary Table S3). Consistent with the intended design of OmoMYC, three out of the four mutations introduced to generate the OmoMYC protein led to additional interactions between the two monomers (Figure 1a,c). The newly introduced hydrogen bonds are formed between two threonine residues (T63) bridged by water molecules as well as the asparagines (N77) of both molecules with an additional interaction to lysine 81 in monomer B. Hydrophobic interactions are observed between two isoleucine residues (I70) and to lysine 66. Further hydrophobic interactions are observed between threonine 63 and leucine 66. Glutamine 76, which is also a mutated residue in OmoMYC, faces away from the interface.

Differences in protein-protein interactions between the OmoMYC homodimer and the MYC/MAX heterodimer are not limited to the mutated residues, but can also be identified

throughout the entire interface (Figure 1c). OmoMYC also displayed a disulfide bridge formed by its penultimate cysteine residues (Figure 1a; Supplementary Figure S1d). Using the 'Protein interfaces, surfaces and assemblies' (PISA) tool[22], we estimated that the protein-protein interface of the OmoMYC homodimer is more stable than the MYC/MAX heterodimer (ΔG=-41 kcal/mol versus -33 kcal/mol; Supplementary Table S4). Heterodimers of OmoMYC with MYC and MAX would contain repulsive interactions or lack stabilizing interactions that would lower their stability (Supplementary Figure S1e-g), suggesting that OmoMYC preferentially forms homodimers.

In the DNA-bound complex, OmoMYC binds to the major groove of the DNA by forming a scissor-like structure at the E-box, which is stabilized via phosphate-backbone interactions and base-specific interactions. The latter are mediated via a histidine (H12), glutamate (E16), arginine (R20) triad in the basic region (Figure 1b; Supplementary Figure S2a,b). A comparison of the protein-DNA interface of OmoMYC to the one of the MYC/MAX DNA complex indicates that the basic region of both complexes assume the same contacts to DNA, suggesting that OmoMYC could compete with MYC/MAX for E-box binding[21] (Supplementary Figure S2c; Supplementary Table S2a,b). We therefore studied the DNA binding properties of all three proteins using a fluorescently labeled oligonucleotide carrying a consensus E-box sequence. Recombinant MAX proteins bound to this sequence with high affinity, whereas binding of MYC was only detectable at micromolar protein concentrations (Figure 2a,b; Supplementary Figure S3a). Consistent with previous results, MAX and MYC co-operated in DNA binding and MYC/MAX complexes bound DNA with a higher affinity than MAX homodimers (Figure 2a,b; Supplementary Figure S3a,b). OmoMYC homodimers bound DNA with an affinity that is even higher than that of MYC/MAX complexes, both in the absence and presence of reducing agent (Figure 2a,b; Supplementary Figure S3a). Furthermore, OmoMYC formed heterodimers with MYC that bound to DNA with an intermediate affinity (Figure 2a,b; Supplementary Figure S3a,b). We were unable to unequivocally ascertain whether OmoMYC/MAX heterodimers bind DNA.

To demonstrate that OmoMYC homodimers exist in cells, we first briefly exposed cells stably expressing OmoMYC to conditions known to oxidize cysteine residues (100 µM H_2O_2, 5 min[23]). Upon treatment of cells with H_2O_2, virtually all OmoMYC molecules migrated with a molecular weight expected of a covalently-linked homodimer in a non-reducing SDS PAGE (Figure 2c). Mutation of the penultimate cysteine to serine (OmoMYC-CS) confirmed that this residue was involved in dimerization under oxidizing conditions (Figure 2c). Second, we stably co-expressed both HA-tagged and FLAG-tagged alleles of OmoMYC in U2OS cells and precipitated lysates with α-FLAG antibodies (Figure 2d). These experiments confirmed that OmoMYC forms homodimers in cells. The cells express a doxycycline-inducible allele of MYC[24] and we also expressed a HA-tagged allele of MYC in cells expressing FLAG-OmoMYC. Probing the immunoprecipitates with α-MYC, α-HA and α-MAX antibodies showed that OmoMYC also forms heterodimers with both MYC and MAX in cells (Figure 2d), consistent with previous results[25]. Notably, doxycycline-mediated induction of wtMYC or expression of HA-MYC significantly reduced binding of OmoMYC to MAX, but had little effect on homodimerization of OmoMYC, arguing that OmoMYC homodimers are more stable than OmoMYC/MYC and OmoMYC/MAX heterodimers (Figure 2d). We concluded that OmoMYC forms stable homodimers and heterodimers with MYC and MAX in cells and that both OmoMYC homodimers and OmoMYC/MYC heterodimers bind specifically to DNA.

OmoMYC blunts promoter invasion by oncogenic MYC levels

To determine how OmoMYC binds to chromatin, we stably expressed HA-tagged OmoMYC in U2OS cells that express a doxycycline-inducible allele of MYC, which we have previously characterized[24] (Figure 3a). We performed chromatin-immunoprecipitation coupled with high-throughput sequencing (ChIP-sequencing) using an α-HA and an α-MYC antibody, which recognizes the amino-terminal 262 amino acids of MYC that are not present in OmoMYC. ChIP results of individual genes and inspection of multiple individual regions of the genome showed that overall binding patterns of MYC and OmoMYC were very similar (Figure 3b,

Supplementary Figure S4a,b). This result was confirmed by a global analysis of all MYC binding sites, which showed a highly significant overlap in binding sites (Figure 3c). Consistent with these findings, *de novo* motif analysis confirmed that OmoMYC binding sites were enriched in both consensus (CACGTG) and non-consensus E-box (CANNTG) binding sites (Supplementary Figure S4c). In addition, OmoMYC, like MYC, showed a preference for promoters and enhancers with an open chromatin structure even in the absence of a cognate binding site[26, 27] (Supplementary Figure S4d,e).

U2OS cells express relatively low levels of endogenous MYC that are identical to levels found in several non-transformed proliferating cell lines; upon doxycycline-induction, levels increase to those found in colon carcinoma and HeLa cells[28]. These "oncogenic" levels of MYC bind to additional sites not occupied by physiological MYC levels ("promoter invasion")[24, 29]. Quantitative analyses show that promoters differ strongly in the MYC concentration at which binding is half-maximal (EC_{50}) and that EC_{50} values stratify functionally different classes of MYC target genes[28]. To test how OmoMYC affects chromatin association of MYC, we performed ChIP-sequencing for MYC at both concentrations in the presence and absence of OmoMYC. Expression of OmoMYC reduced binding of MYC at both promoters and non-promoter binding sites (Figure 3d). Consistent with its molecular properties, the decrease in MYC binding caused by OmoMYC was stronger on consensus E-box sequences than on non-consensus E-boxes or on binding sites that lacked an E-box (Figure 3d, Supplementary Figure S5a).

Importantly, the decrease in MYC binding was not uniform for all promoters. Rather, OmoMYC had little influence on MYC binding at promoters that are highly occupied by physiological levels of MYC and to which no additional MYC is recruited when MYC levels increase to supra-physiological levels (Figure 3e). In contrast, OmoMYC decreased the recruitment of MYC ("invasion") to promoters upon doxycycline induction (Figure 3e). Indeed, the effect of OmoMYC on MYC binding correlated with the EC_{50} values for the respective gene (Supplementary Figure S5b). One way to rationalize these findings is the suggestion that OmoMYC competes with MYC/MAX complexes for binding to DNA. MYC/MAX binding

at promoters that are highly occupied by physiological MYC levels is stabilized by protein/protein interactions of the MYC amino-terminus that is not present in OmoMYC and therefore are not competed by OmoMYC (see Discussion and Figure 8)[28].

OmoMYC attenuates oncogenic MYC-dependent gene expression

RQ-PCR analyses showed that expression of OmoMYC interferes significantly with induction of individual genes by MYC (Figure 4a). To obtain a global picture of OmoMYC-dependent gene regulation, we performed RNA-sequencing in the presence and absence of OmoMYC without and 30 h after induction of ectopic MYC expression. The analysis showed that OmoMYC significantly attenuated both transcriptional activation and repression by MYC (Figure 4b).

We have previously shown that the change in expression of a given gene in response to doxycycline-mediated induction of MYC correlates with the change in occupancy of its promoter[24, 28]. Consistent with the DNA binding data, attenuation of gene regulation by OmoMYC was not uniform but was strongest on genes that respond to an increase from physiological to supra-physiological level of MYC (Figure 4c, red). The simplest model to account for this observation is that OmoMYC competes with MYC/MAX complexes on DNA to lower MYC/MAX affinity to its cognate binding sites and thereby blunts the "invasion" of low affinity promoters. In support of this notion, we found that the OmoMYC-dependent change in expression correlated with the decrease in MYC binding over all MYC target genes (Figure 4d).

To test if specific DNA-binding is required for OmoMYC's effects on gene regulation, we stably expressed two alleles of OmoMYC: one OmoMYC(HER), in which the DNA-binding triad in the basic region H12-E16-R20 is mutated to alanine and a second, which carried alanine substitutions only at H12 and E16 (OmoMYC(HE)), since mutation of the two homologous residues in MYC (H359A-E363A) is sufficient to abolish specific E-box recognition (B. Amati, personal communication). We confirmed that both OmoMYC(HER) and OmoMYC(HE) accumulate in the nucleus upon stable expression in cells

(Supplementary Figure S6a,b). ChIP experiments confirmed that both OmoMYC(HER) and OmoMYC(HE) are compromised in their ability to recognize target promoters on DNA (Figure 4e). Analysis of individual genes showed that both OmoMYC(HE) and OmoMYC(HER) are severely compromised in their ability to inhibit MYC-dependent transcription (Figure 4f). This was confirmed by RNA-sequencing, which showed that mutation of the basic region largely, but not completely abolished the repressive effect of OmoMYC on MYC-dependent transcription (Figure 4c, Supplementary Figure S6c). Collectively, the data argue that the predominant mode, by which OmoMYC inhibits MYC-dependent gene regulation, is the formation of DNA binding-homodimers that compete with MYC/MAX heterodimers for their target DNA.

OmoMYC-regulated genes define a signature characteristic of multiple MYC-driven tumors
GSE analyses showed that OmoMYC reverted expression of multiple well-characterized MYC target gene signatures (Figure 5a). This suggested that OmoMYC might blunt an expression program that is characteristic of human tumors characterized by high MYC expression. GSE analyses showed that this is indeed the case and that OmoMYC target genes identify tumors with high MYC levels in human neuroblastoma, multiple myeloma, medulloblastoma, colon carcinoma, and Burkitt lymphoma (Figure 5b,c). Notably, the most consistent overlap was observed for genes that are repressed by OmoMYC, which largely correspond to genes that are activated by MYC. While OmoMYC-activated (MYC-repressed) genes discriminated medulloblastomas and multiple myelomas with high MYC levels, they did not reliably identify colon carcinoma and human Burkitt lymphoma, possibly indicating that direct repression by MYC is not a predominant mode of gene regulation in these entities. Consistent with this notion and the human data, OmoMYC-repressed genes, but not OmoMYC-activated genes, discriminated both pre-tumoral stages from control lymphocytes and also frank lymphomas from pre-tumoral stages in mouse models of MYC-driven lymphomagenesis[7] (Figure 5d). In contrast, sets of high affinity MYC target genes that are not competed or regulated by OmoMYC discriminated normal B-cells from both pre-

lymphomagenic cells and lymphomas, but were unable to discriminate pre-lymphomagenic cells from frank lymphomas (Supplementary Figure S7a). Furthermore, OmoMYC had little effect on expression of genes regulated by endogenous MYC during mitogenic stimulation of fibroblasts (Figure 5e). OmoMYC-regulated genes also discriminated pancreatic carcinomas with high MYC expression and particularly bad prognosis from less aggressive carcinomas (Supplementary Figure S7b). We concluded that OmoMYC regulates a group of MYC target genes that is characteristic of tumor entities expressing high levels of MYC across multiple entities.

Identification of OmoMYC target genes critical for growth of MYC-dependent tumor cells

GSE analysis of the OmoMYC-regulated genes revealed a spectrum of functions that have been identified in previous analyses of MYC target genes[1] (Supplementary Figure S8a). We therefore performed a targeted shRNA screen to identify candidate genes that can explain the ability of OmoMYC to specifically interfere with tumor cell growth. Cultures of U2OS cells expressing OmoMYC revealed rapid selection against the ectopically expressed OmoMYC, which precluded the analysis of effects of OmoMYC on cell growth (L.A.J., unpublished observation). We therefore used an inducible allele to analyze OmoMYC function in cells derived from KRAS-driven pancreatic tumors, since previous work had established that MYC levels and function are critical for growth of these tumors *in vivo*[24]. We generated cell lines that express OmoMYC in a doxycycline-inducible manner in KRAS/p53^{mut} cells (KPC) (Figure 6a). OmoMYC suppressed both adherent and anchorage-independent growth of KPCs (Figure 6b, Supplementary Figure S8b,c). RNA-sequencing showed that genes regulated by OmoMYC in KPCs are highly similar to those regulated in U2OS cells (Supplementary Figure S8d).

We next generated a focused shRNA library that targets genes that are activated by MYC and repressed by OmoMYC (Figure 6c, Supplementary Table S5). Each of the genes was covered by five shRNAs, and the representation of individual shRNAs was determined by high-throughput sequencing after 4 days of induction. This focused screen identified three

significant hits, BOP1, RPN13 (also known as ADRM1) and ATAD3A (Figure 6d, Supplementary Table S6). Both MYC and OmoMYC bound to the promoters of BOP1 and ATAD3A confirming they are direct targets of both (Supplementary Figure S9a,b). Like the entire set of OmoMYC-regulated genes, expression of all three genes correlated with MYC expression in several human tumor entities (Supplementary Figure S9c). Independent work had established that expression of each of these genes is enhanced in multiple human tumors and can be prognostic for tumor outcome[30-33]. Indeed, inhibitors of ribosome biogenesis (e.g. of RNA Polymerase I) and inhibitors of ADRM1 are currently being explored for tumor therapy[32, 34]. We confirmed that both inhibitors of RNA Polymerase I (CX-5461) and of ADRM1 (RA 190) suppress growth of KPCs, validating the results of the screen (Figure 6e). Titration of both inhibitors revealed no evidence for synergy, consistent with the fact that they inhibit independent cell biological processes (Supplementary Figure S9d).

The most significant hit in this screen is ATAD3A, a protein that promotes fusion of mitochondria[35]. ATAD3A is a downstream target of the mTOR pathway and required for cell growth in *Drosophila* and *Caenorhabditis elegans*[35, 36]. Consistent with these observations and the screening results, shRNA-mediated depletion of ATAD3A attenuated growth of KPCs (Figure 6f,g). We confirmed that ATAD3A localizes to mitochondria (Figure 7a). Changes in mitochondrial dynamics alter mitochondrial metabolism in response to cell growth and metabolism. We speculated that uncoupling of both processes might lead to the accumulation of reactive oxygen species (ROS). In support of this notion, shRNA-mediated suppression of ATAD3A using two shRNAs caused an increase in mitochondrial ROS that correlated with the decrease in ATAD3A expression (Figure 7b,d). Depletion of PLD6, a MYC-induced gene that encodes a phospholipase that initiates mitochondrial fusion also sharply increased ROS levels in mitochondria, supporting the notion that this increase is due to altered mitochondrial dynamics[37] (Figure 7c). Maintaining a redox balance is of particular importance for transformed cells due to a prevalence of anabolic processes that consume reducing equivalents. Indeed, depletion of ATDA3A caused MYC-dependent apoptosis in

U2OS cells (Figure 7e). We concluded that ATAD3A-dependent changes in mitochondrial

dynamics are critical for the survival of cells that express high levels of MYC.

Discussion

Here, we have solved the structure and studied the properties of OmoMYC to understand how OmoMYC can discriminate between physiological and oncogenic functions of MYC. Consistent with the intended design, we find that OmoMYC forms homodimers that are stabilized by interactions of residues that are mutated in OmoMYC[20]. The overall structure of OmoMYC (including the DNA binding domain) is highly similar to the structures of other HLH/Zip proteins. OmoMYC homodimers interact with DNA in the same manner as MAX homodimers and MYC/MAX heterodimers[21, 38]. This suggests a model, in which OmoMYC competes with MYC/MAX complexes for binding to DNA, and is in line with previous observations that ectopically expressed OmoMYC can be chromatin-immunoprecipitated at MYC target sites[25]. In support of this model, we found that mutant alleles of OmoMYC with reduced affinity to E-box containing DNA are compromised in their ability to antagonize MYC-dependent gene expression. We confirm previous findings that OmoMYC forms heterodimers with MYC and MAX [25], although both estimation of heterodimer stability from the crystal structure and immunoprecipitation experiments from cells suggest that OmoMYC/MYC and OmoMYC/MAX heterodimers have lower stabilities than OmoMYC homodimers. OmoMYC/MYC heterodimers are capable of binding to DNA. Therefore the reduction in chromatin association of MYC caused by OmoMYC homodimers is attenuated by formation of OmoMYC/MYC heterodimers. Furthermore, it is possible, that OmoMYC/MYC heterodimers regulate transcription similar to MYC/MAX heterodimers. If this is the case, the biological effects of OmoMYC are attenuated by OmoMYC/MYC heterodimers, implying that the design of more potent OmoMYC alleles is possible that shift the dimerization balance towards even more stable homodimer formation.

OmoMYC competes with MYC/MAX heterodimers on chromatin and thereby reduces their occupancy at cognate binding sites. OmoMYC blunts the binding of MYC to low affinity sites ("promoter invasion") that is characteristic of the high levels of MYC observed in many human tumors, but has a significantly weaker effect on MYC binding to sites bound by

physiological MYC levels (Figure 8). We hypothesize that the ability of OmoMYC to discriminate different classes of target genes is due to the fact that MYC binding to promoters with an apparent high affinity is stabilized by local protein/protein interactions in addition to contacts with DNA (Figure 8)[28]. This suggestion is supported by the recent identification of core promoter factors that bind to MYC and stabilize its binding to promoters and by biochemical and mathematical modeling analyses arguing that both binding of MYC to DNA and to promoter–bound factors is required to account for the chromatin binding behavior of MYC in cells [27, 28, 39, 40]. Many expression profiles have been identified that are characteristic for tumor entities or subgroups that express particularly high MYC or N-MYC levels. OmoMYC reverts a MYC-dependent gene expression program that is recognizable in multiple human and mouse tumor entities, providing a model how it can have broad anti-tumor activity. At the same time, OmoMYC has significantly less effect on gene expression programs of normal proliferating cells, correlating with its low toxicity *in vivo*.

Genes that responded particularly strongly to OmoMYC did not encode proteins that are functionally linked to one specific cellular process. We therefore performed an shRNA screen to identify downstream targets via which OmoMYC may suppress tumor cell growth. The screen identified BOP1, which is part of a trimeric complex ("PeBoW") that is essential for processing and maturation of mammalian 5.8S and 28S ribosomal RNAs[41], ADRM1 (also known as RPN13), an ubiquitin acceptor on the proteasome[42] and ATAD3A, a calcium-regulated protein involved in mitochondrial dynamics and transport from the ER to the mitochondrion[35, 43]. Ribosome biogenesis and protein translation are essential for normal cell growth. Nevertheless, both processes are enhanced to supra-physiological levels in MYC-driven tumors and targeting these processes opens specific therapeutic windows[16, 44]. Likewise, targeting ADRM1 using small molecule inhibitors opens a wide therapeutic window between normal and tumor cells[32]. Similarly, we find that cells expressing high levels of MYC have an enhanced dependence on ATAD3A for survival, suggesting that targeting ATAD3A may also be effective against MYC-dependent tumor cells. ATAD3A has anti-apoptotic

functions in tumors, potentially via its effects on mitochondrial dynamics[33, 45]. Collectively, our findings suggest that individual genes encoding rate-limiting proteins involved in basic cell biological processes respond to the difference between physiological and supra-physiological MYC levels and that OmoMYC specifically inhibits tumor cell growth since it suppresses expression of this group of genes. A similar picture has emerged from studies of nucleotide biosynthesis genes: despite pervasive binding of MYC to promoters of nucleotide biosynthetic enzymes[46], deregulation of a single rate-limiting enzyme, phosphoribosyl-pyrophosphate synthetase 2 (PRPS2), promotes the increased nucleotide biosynthesis of MYC-transformed cells[47]. A complete understanding of how to mimic OmoMYC´s efficacy with small molecule inhibitors will therefore require an analysis of its target genes in an *in vivo* setting.

Materials and methods

A detailed description of all materials and methods can be found in the Supplementary Information.

Expression and purification of recombinant OmoMYC, MYC and MAX protein

OmoMYC, MYC (aa353-434) and MAX were expressed as N-terminally His-tagged or GST-tagged proteins in *E.coli* and chromatographically purified using the ÄKTA protein purification systems (GE Healthcare, Chicago, IL, USA).

Crystallization of OmoMYC

OmoMYC apo crystals were grown using the vapor diffusion method in sitting drops and analyzed at beamline ID23-1 at the ESRF (Grenoble, France) to a resolution of 1.95 Å. The DNA-bound OmoMYC complex was generated by crystallizing his-tagged OmoMYC in the presence of an E-box oligonucleotide[38]. The data set was collected at beamline 14.1 (BESSY II, Berlin, Germany) to a resolution of 2.7 Å. The structures were solved via Phaser by molecular replacement using the MYC/MAX dimer (1NKP)[21] as initial search model. PDB codes for OmoMYC are: 5I4Z (apo structure) and 5I50 (DNA-bound structure).

Gel mobility shift assays

Increasing concentrations of recombinant OmoMYC, MAX and MYC were used for binding reactions with a double stranded, 5'CY3 labeled DNA substrate (CM1)[48]. Where indicated, antibodies were added prior to DNA addition. K_d values were calculated using Prism (GraphPad Software, La Jolla, CA, USA) assuming complete dimer formation with a four parameter non-linear regression.

Cell culture

U2OS tet-on-*MYC* cells[24] and KPCs (Ptf1a+/Cre;Kras+/LSL-G12D;p53loxP/R172H) were cultured according to standard conditions; U2OS were authenticated via STR Analysis; KPCs

were a kind gift of Jens Siveke (Technical University of Munich, Germany). All cell lines were routinely tested for mycoplasma contamination.

Pooled negative-selection shRNA screening

A custom shRNA library directed against OmoMYC target genes (Supplementary Table S5) was cloned into the inducible lentiviral vector RT3GEPIR[49]. KPC cells were transduced with the pooled library and cultivated in the presence or absence of doxycycline for four days. shRNA sequences were PCR recovered from genomic DNA of harvested cells and changes in shRNA frequencies were determined by next-generation sequencing with an Illumina GAIIx (Illumina, San Diego, CA, USA).

Bioinformatic analysis and statistics

Information on data processing for ChIP- and RNA-sequencing is at GEO: GSE77328. For binned data the mean of each bin is plotted. Sorting of the binned data was done using independent experiments. Regression lines were estimated using linear models and corresponding p-values were calculated using 2-tailed t-distribution. Statistical significant differences between two regression lines were determined using an analysis of covariances (ANCOVA). p-values for box plots were calculated with non-parametric 2-tailed Wilcoxon-Mann-Whitney tests.

Conflict of interest

The authors declare no competing financial interests.

Availability of data

High-throughput-sequencing data are available at the Gene Expression Omnibus under the accession number GEO: GSE77328. Reviewers can access the data via:

http://www.ncbi.nlm.nih.gov/geo/query/acc.cgi?token=ihadcouozbapxif&acc=GSE77328.

Atomic coordinates have been prepared for deposition in the Protein Data Bank under accession codes 5I4Z (apo structure) and 5I50 (DNA-bound structure).

Supplementary Information

Supplementary Information accompanies the paper on the *Oncogene* website (http://www.nature.com/onc).

References

1   Dang CV. MYC on the path to cancer. Cell 2012; 149: 22-35.

2   Kress TR, Sabo A, Amati B. MYC: connecting selective transcriptional control to global RNA production. Nat Rev Cancer 2015; 15: 593-607.

3   Wolf E, Lin CY, Eilers M, Levens DL. Taming of the beast: shaping Myc-dependent amplification. Trends Cell Biol 2015; 25: 241-248.

4   Shen-Li H, O'Hagan RC, Hou H, Jr., Horner JW, 2nd, Lee HW, DePinho RA. Essential role for Max in early embryonic growth and development. Genes & development 2000; 14: 17-22.

5   Scognamiglio R, Cabezas-Wallscheid N, Thier MC, Altamura S, Reyes A, Prendergast AM *et al*. Myc Depletion Induces a Pluripotent Dormant State Mimicking Diapause. Cell 2016; 164: 668-680.

6   Laurenti E, Varnum-Finney B, Wilson A, Ferrero I, Blanco-Bose WE, Ehninger A *et al*. Hematopoietic stem cell function and survival depend on c-Myc and N-Myc activity. Cell stem cell 2008; 3: 611-624.

7   Sabo A, Kress TR, Pelizzola M, de Pretis S, Gorski MM, Tesi A *et al*. Selective transcriptional regulation by Myc in cellular growth control and lymphomagenesis. Nature 2014; 511: 488-492.

8   Kress TR, Cannell IG, Brenkman AB, Samans B, Gaestel M, Roepman P *et al*. The MK5/PRAK kinase and Myc form a negative feedback loop that is disrupted during colorectal tumorigenesis. Mol Cell 2011; 41: 445-457.

9   Sodir NM, Swigart LB, Karnezis AN, Hanahan D, Evan GI, Soucek L. Endogenous Myc maintains the tumor microenvironment. Genes & development 2011; 25: 907-916.

10   Giuriato S, Ryeom S, Fan AC, Bachireddy P, Lynch RC, Rioth MJ *et al*. Sustained regression of tumors upon MYC inactivation requires p53 or thrombospondin-1 to reverse the angiogenic switch. Proceedings of the National Academy of Sciences of the United States of America 2006; 103: 16266-16271.

11   Dang CV, Kim JW, Gao P, Yustein J. The interplay between MYC and HIF in cancer. Nat Rev Cancer 2008; 8: 51-56.

12   Reimann M, Lee S, Loddenkemper C, Dörr JR, Tabor V, Aichele P *et al*. Tumor Stroma-Derived TGF-β Limits Myc-Driven Lymphomagenesis via Suv39h1-Dependent Senescence. Cancer cell 2010; 17: 262-272.

13   van Riggelen J, Muller J, Otto T, Beuger V, Yetil A, Choi PS *et al*. The interaction between Myc and Miz1 is required to antagonize TGFbeta-dependent autocrine signaling during lymphoma formation and maintenance. Genes & development 2010; 24: 1281-1294.

14   Lawson DA, Bhakta NR, Kessenbrock K, Prummel KD, Yu Y, Takai K *et al*. Single-cell analysis reveals a stem-cell program in human metastatic breast cancer cells. Nature 2015; 526: 131-135.

15   Truitt ML, Conn CS, Shi Z, Pang X, Tokuyasu T, Coady AM *et al*. Differential Requirements for eIF4E Dose in Normal Development and Cancer. Cell 2015; 162: 59-71.

16   Barna M, Pusic A, Zollo O, Costa M, Kondrashov N, Rego E *et al*. Suppression of Myc oncogenic activity by ribosomal protein haploinsufficiency. Nature 2008; 456: 971-975.

17   Soucek L, Whitfield J, Martins CP, Finch AJ, Murphy DJ, Sodir NM *et al*. Modelling Myc inhibition as a cancer therapy. Nature 2008; 455: 679-683.

18   Annibali D, Whitfield JR, Favuzzi E, Jauset T, Serrano E, Cuartas I *et al*. Myc inhibition is effective against glioma and reveals a role for Myc in proficient mitosis. Nat Commun 2014; 5: 4632.

19   Soucek L, Whitfield JR, Sodir NM, Masso-Valles D, Serrano E, Karnezis AN *et al*. Inhibition of Myc family proteins eradicates KRas-driven lung cancer in mice. Genes & development 2013; 27: 504-513.

20   Soucek L, Helmer-Citterich M, Sacco A, Jucker R, Cesareni G, Nasi S. Design and properties of a Myc derivative that efficiently homodimerizes. Oncogene 1998; 17: 2463-2472.

21   Nair SK, Burley SK. X-ray structures of Myc-Max and Mad-Max recognizing DNA. Molecular bases of regulation by proto-oncogenic transcription factors. Cell 2003; 112: 193-205.

22   Krissinel E, Henrick K. Inference of macromolecular assemblies from crystalline state. J Mol Biol 2007; 372: 774-797.

23   Abate C, Patel L, Rauscher FJ, 3rd, Curran T. Redox regulation of fos and jun DNA-binding activity in vitro. Science 1990; 249: 1157-1161.

24   Walz S, Lorenzin F, Morton J, Wiese KE, von Eyss B, Herold S *et al*. Activation and repression by oncogenic MYC shape tumour-specific gene expression profiles. Nature 2014; 511: 483-487.

25   Savino M, Annibali D, Carucci N, Favuzzi E, Cole MD, Evan GI *et al*. The action mechanism of the Myc inhibitor termed Omomyc may give clues on how to target Myc for cancer therapy. PLoS One 2011; 6: e22284.

26   Guccione E, Martinato F, Finocchiaro G, Luzi L, Tizzoni L, Dall' Olio V *et al*. Myc-binding-site recognition in the human genome is determined by chromatin context. Nature cell biology 2006; 8: 764-770.

27   Guo J, Li T, Schipper J, Nilson KA, Fordjour FK, Cooper JJ *et al*. Sequence specificity incompletely defines the genome-wide occupancy of Myc. Genome Biol 2014; 15: 482.

28   Lorenzin F, Benary U, Jung LA, von Eyß B, Walz S, Kisker C *et al*. Promoter affinity is a critical determinant of the specific gene expression patterns elicited by different MYC levels. eLife 2016; in press.

29   Lin CY, Loven J, Rahl PB, Paranal RM, Burge CB, Bradner JE *et al*. Transcriptional Amplification in Tumor Cells with Elevated c-Myc. Cell 2012; 151: 56-67.

30   Killian A, Sarafan-Vasseur N, Sesboue R, Le Pessot F, Blanchard F, Lamy A *et al*. Contribution of the BOP1 gene, located on 8q24, to colorectal tumorigenesis. Genes Chromosomes Cancer 2006; 45: 874-881.

31   Chung KY, Cheng IK, Ching AK, Chu JH, Lai PB, Wong N. Block of proliferation 1 (BOP1) plays an oncogenic role in hepatocellular carcinoma by promoting epithelial-to-mesenchymal transition. Hepatology 2011; 54: 307-318.

32   Anchoori RK, Karanam B, Peng S, Wang JW, Jiang R, Tanno T *et al*. A bis-benzylidine piperidone targeting proteasome ubiquitin receptor RPN13/ADRM1 as a therapy for cancer. Cancer cell 2013; 24: 791-805.

33   Fang HY, Chang CL, Hsu SH, Huang CY, Chiang SF, Chiou SH *et al*. ATPase family AAA domain-containing 3A is a novel anti-apoptotic factor in lung adenocarcinoma cells. Journal of cell science 2010; 123: 1171-1180.

34   Bywater MJ, Poortinga G, Sanij E, Hein N, Peck A, Cullinane C *et al*. Inhibition of RNA polymerase I as a therapeutic strategy to promote cancer-specific activation of p53. Cancer cell 2012; 22: 51-65.

35   Gilquin B, Taillebourg E, Cherradi N, Hubstenberger A, Gay O, Merle N *et al*. The AAA+ ATPase ATAD3A controls mitochondrial dynamics at the interface of the inner and outer membranes. Molecular and cellular biology 2010; 30: 1984-1996.

36   Hoffmann M, Bellance N, Rossignol R, Koopman WJ, Willems PH, Mayatepek E *et al*. C. elegans ATAD-3 is essential for mitochondrial activity and development. PLoS One 2009; 4: e7644.

37   von Eyss B, Jaenicke LA, Kortlever RM, Royla N, Wiese KE, Letschert S *et al*. A MYC-Driven Change in Mitochondrial Dynamics Limits YAP/TAZ Function in Mammary Epithelial Cells and Breast Cancer. Cancer cell 2015; 28: 743-757.

38   Ferré D'Amaré AR, Prendergast GC, Ziff EB, Burley SK. Recognition by Max of its cognate DNA through a dimeric b/HLH/Z domain. Nature 1993; 363: 38-45.

39   Thomas LR, Wang Q, Grieb BC, Phan J, Foshage AM, Sun Q *et al*. Interaction with WDR5 promotes target gene recognition and tumorigenesis by MYC. Mol Cell 2015; 58: 440-452.

40   Jaenicke LA, von Eyss B, Carstensen A, Wolf E, Xu W, Greifenberg AK *et al*. Ubiquitin-Dependent Turnover of MYC Antagonizes MYC/PAF1C Complex Accumulation to Drive Transcriptional Elongation. Mol Cell 2016; 61: 54-67.

41   Rohrmoser M, Holzel M, Grimm T, Malamoussi A, Harasim T, Orban M *et al*. Interdependence of Pes1, Bop1, and WDR12 controls nucleolar localization and assembly of the PeBoW complex required for maturation of the 60S ribosomal subunit. Molecular and cellular biology 2007; 27: 3682-3694.

42   Husnjak K, Elsasser S, Zhang N, Chen X, Randles L, Shi Y *et al*. Proteasome subunit Rpn13 is a novel ubiquitin receptor. Nature 2008; 453: 481-488.

43   Chiang SF, Huang CY, Lin TY, Chiou SH, Chow KC. An alternative import pathway of AIF to the mitochondria. Int J Mol Med 2012; 29: 365-372.

44   Ruggero D. Translational control in cancer etiology. Cold Spring Harbor perspectives in biology 2013; 5.

45   Huang KH, Chow KC, Chang HW, Lin TY, Lee MC. ATPase family AAA domain containing 3A is an anti-apoptotic factor and a secretion regulator of PSA in prostate cancer. Int J Mol Med 2011; 28: 9-15.

46   Liu YC, Li F, Handler J, Huang CR, Xiang Y, Neretti N *et al*. Global regulation of nucleotide biosynthetic genes by c-Myc. PLoS ONE 2008; 3: e2722.

47   Cunningham JT, Moreno MV, Lodi A, Ronen SM, Ruggero D. Protein and nucleotide biosynthesis are coupled by a single rate-limiting enzyme, PRPS2, to drive cancer. Cell 2014; 157: 1088-1103.

48   Blackwell TK, Kretzner L, Blackwood EM, Eisenman RN, Weintraub H. Sequence-specific DNA binding by the c-myc protein. Science 1990; 250: 1149-1151.

49   Fellmann C, Hoffmann T, Sridhar V, Hopfgartner B, Muhar M, Roth M *et al*. An optimized microRNA backbone for effective single-copy RNAi. Cell reports 2013; 5: 1704-1713.

50   Subramanian A, Tamayo P, Mootha VK, Mukherjee S, Ebert BL, Gillette MA *et al*. Gene set enrichment analysis: a knowledge-based approach for interpreting genome-wide expression profiles. Proceedings of the National Academy of Sciences of the United States of America 2005; 102: 15545-15550.

51   Perna D, Faga G, Verrecchia A, Gorski MM, Barozzi I, Narang V *et al*. Genome-wide mapping of Myc binding and gene regulation in serum-stimulated fibroblasts. Oncogene 2012; 31: 1695-1709.

Figure Legends

Figure 1: Structure and DNA-binding properties of OmoMYC.

(a) Schematic representation of the apo OmoMYC crystal structure. Mutations that distinguish OmoMYC from MYC are highlighted in red. Boxes on the right highlight the carboxy-terminal disulfide bridge (top), the hydrogen bond network involving N77 (middle) and hydrogen bonds bridged by two water molecules between T63 (bottom). Images were generated using PyMOL. (b: basic region; HLH: helix-loop-helix region; Zip: leucine zipper).

(b) Crystal structure of the OmoMYC homodimer bound to a consensus E-box. The CACGTG motif is highlighted in blue. The boxes on the right illustrate base-specific interactions of one arm of the OmoMYC homodimer (green) to one half of the palindromic E-box sequences of the double-stranded DNA (grey). For comparison, base-specific protein-DNA contacts of MYC in the MYC/MAX structure (1NKP)[21] are illustrated in the upper box.

(c) Interactions that distinguish the OmoMYC homodimer (upper panel) from the MYC/MAX heterodimer (lower panel) as deduced from the crystal structures. Mutations of OmoMYC relative to MYC are shown as red dots. Dotted lines indicate interactions of the carboxy-terminus (boxed), which is not present in the MYC/MAX crystal structure and can therefore not be compared reliably. IA: interaction.

Figure 2: OmoMYC preferentially forms homodimers and binds to DNA *in vitro*.

(a) Electrophoretic mobility shift assays (EMSAs) comparing binding of MAX, MYC/MAX, OmoMYC and MYC/OmoMYC dimers to a consensus E-box oligonucleotide. Protein concentrations (calculated as dimers) are indicated. The upper band shows protein-bound Cy3-labeled DNA (bound DNA) while the lower band reflects unbound labeled DNA (free DNA). Protein concentrations are shown for dimers. (n≥3; n indicates the number of independent biological replicates.)

(b) Determination of dissociation constants (K_d) of the protein-DNA complexes from EMSAs as shown in panel (a). Fractions of bound DNA (% bound) were plotted against the logarithmic protein concentration (c_{prot}) (n≥3). Error bars indicate SEM. K_d values obtained by a four parameter non-linear fit using GraphPad Prism are shown in the table to the right. CI: confidence interval.

(c) U2OS cells stably expressing HA-tagged OmoMYC or a mutant allele, in which the penultimate cysteine (C91) was replaced by a serine were treated with 100 μM H_2O_2 where indicated. SDS-PAGE was performed under reducing or non-reducing conditions (± DTT) and blots probed with an α-HA antibody. CDK2 was used as a loading control (n=4). *: non-specific bands, upper arrow: covalently linked dimer, lower arrow: monomer, vec: empty vector control, Omo: HA-OmoMYC, CS: HA-OmoMYC(CS) mutant.

(d) Immunoprecipitation of FLAG-tagged OmoMYC with α-FLAG antibody in U2OS cells expressing exogenous HA-tagged OmoMYC or MYC (HA-tagged or doxycycline-induced untagged). Co-immunoprecipitated proteins were compared to 8 % (α-FLAG and α-MYC immunoblots) or 4 % (α-HA and α-MAX immunoblots) input material (n=3). *: heavy chain, DOX: doxycycline, vec: empty vector control.

Figure 3: OmoMYC attenuates chromatin binding of MYC.

(a) Immunoblot showing doxycycline-mediated MYC expression in U2OS cells and in U2OS cells expressing OmoMYC. Where indicated, cells were treated with doxycycline (1 μg/ml; 8 h). Lysates were probed with α-MYC, α-HA and α-CDK2 antibodies as indicated (n=3).

(b) Examples for ChIP-sequencing tracks at the *NPM1* and *ARC* loci. ChIP-sequencing was performed with the indicated antibodies from control cells or cells expressing HA-OmoMYC (both U2OS) before or after addition of doxycycline (1 μg/ml; 8 h). Input and HA-ChIP-OmoMYC traces are shown as controls.

(c) Heat maps comparing binding of MYC and OmoMYC proteins to chromatin. MYC peaks were split into peaks close to RNA polymerase II transcribed genes and intergenic

regions. Shown is a window of ±5 kb surrounding the MYC binding sites. Loci are ranked according to MYC occupancy.

(d) Tag density plots comparing MYC binding to core promoters (top, n=1 868) and to non-promoter binding sites (bottom, n=2 543) in the presence and absence of OmoMYC. Traces are shown for MYC binding before (endogenous MYC) and after addition of doxycycline. Only binding sites with consensus E-box sequences are shown.

(e) Diagram demonstrating reduced "invasion" by oncogenic MYC levels in the presence of OmoMYC. All directly bound promoters (n=7 379) were binned into 25 bins according to recruitment of MYC in an independent experiment[24]. The x-axis shows recruitment in the absence, y-axis in the presence of OmoMYC. The p-value was calculated using a linear model and a t-test with an offset of 1. MYC recruitment was calculated by counting the number of tags in a region of +/-100 bp around the summit of the MYC peak, input was subtracted and a fold change between +DOX and -DOX was calculated.

Figure 4: OmoMYC attenuates oncogenic MYC-dependent gene expression.

(a) RQ-PCR assays documenting expression of *CAMKV* after doxycycline-mediated induction of MYC (1 μg/ml; 8 h) in control U2OS cells and in cells constitutively expressing HA-OmoMYC. Error bars indicate SD of technical triplicates (n=3).

(b) Box plots documenting globally attenuated activation and repression by MYC in the presence of OmoMYC in U2OS cells. Left plot shows absolute values for all significantly MYC regulated genes (FDR<0.05), plots on the right show the effect of OmoMYC on MYC activation and repression. The box plots encompass data points between the first and third quartiles. A horizontal line indicates the median, whiskers extend to 1.5x interquartile range and outliers are not shown. The p-values were calculated using two-sided, paired Wilcoxon signed rank tests.

(c) Correlation of MYC-dependent gene regulation in U2OS control cells (x-axis) and in U2OS cells expressing either OmoMYC or OmoMYC (HE) (y-axis). Shown are the $\log_2$ fold-change (FC) values of gene regulation in cells after doxycycline-mediated induction

of MYC (1 μg/ml; 30 h). All expressed genes were sorted for MYC-regulation according to an independent dataset and binned into 38 bins with 490 genes each. A linear model was used to calculate regression lines for binned data of OmoMYC and OmoMYC(HE) expressing cells. r: Pearson correlation coefficient.

(d) Correlation of OmoMYC-dependent change in gene expression with change in promoter occupancy by MYC. All MYC-bound promoters were binned into 17 bins with 400 genes each and sorted for expression changes upon MYC-induction. The p-value indicated significance of linear correlation and was calculated with a two-tailed Student's t-test.

(e) qPCR analysis of a ChIP experiment performed in U2OS cells expressing HA-OmoMYC, one of the two alleles of OmoMYC (HER-AAA or HE-AA) or empty vector (vec). Primer pairs are located in the promoter regions of *NPM1*, *NCL*, *FBXW8*, *CAMKV* and in an intergenic region (Ctr). Error bars are showing SD of technical triplicates (n=2).

(f) RQ-PCR assays documenting expression of *CAMKV* after doxycycline-mediated induction of MYC (1 μg/ml; 30 h) in control cells and in cells constitutively expressing OmoMYC, OmoMYC(HER) or OmoMYC(HE). Error bars indicate SD of technical triplicates (n=6).

Figure 5: OmoMYC reverts MYC-dependent gene expression programs of human and murine tumors.

(a) The panels show gene set enrichment analyses (GSEA) of genes regulated in response to doxycycline-mediated MYC induction and of OmoMYC-regulated genes in U2OS cells. Shown are normalized enrichment scores (NES) and q-values of well-characterized MYC-activated and -repressed gene sets. GSE analyses were performed with signal2noise metric, 1000 permutations and the C2 gene set collection of MSigDB[50].

(b) GSE analysis of three gene sets containing OmoMYC-repressed (n=383), OmoMYC-activated (n=137) and MYC-activated & OmoMYC-repressed (n=148) genes comparing gene expression of stage 4 versus stage 1-3 neuroblastomas (GSE16476).

(c) GSEA of gene expression changes of different human tumors characterized by high MYC or MYCN expression. Expression data from human tumors are sets GSE16476, GSE37382, GSE4475, GSE26760, and GSE39582.

(d) GSEA of different stages of a mouse model of B-cell lymphomagenesis. Expression data from murine Eμ-MYC tumors are from data set GSE51008.

(e) GSEA of gene expression changes in murine embryonic fibroblasts (MEF) in which MYC-activation[7] or MYC-knockout[51] is induced by 4-OHT treatment. Gene sets are defined as in b.

Figure 6: Identification of critical OmoMYC target genes.

(a) Immunoblot of doxycycline-mediated OmoMYC expression in KPCs. Where indicated, cells were treated with doxycycline (1 μg/ml) for 48 h. Lysates were probed with α-HA and α-CDK2 antibodies (n=3).

(b) Analysis of cell growth in KPCs expressing either control vector (vec) or doxycycline-inducible OmoMYC. Where indicated, were grown in the presence of doxycycline (1 μg/ml). Cells were seeded at equal densities and either counted after 3 days (upper part) or stained with crystal violet after 5 days of growth (lower part). Data are presented as mean ±SD of biological triplicates. p-values were calculated using a paired two-tailed Student's t-test.

(c) Flow chart showing the selection process of target genes for a focused shRNA screen. From all expressed genes (RPKM>1), those genes were selected that are significantly activated by doxycycline-induced MYC expression and simultaneously repressed by OmoMYC expression in doxycycline treated cells. These genes were further filtered for druggability (Supplementary Table S5).

(d) Results of the targeted shRNA-screen in KPC cells. Waterfall plots documenting z-scores for $\log_2$FC in shRNA frequencies between doxycycline treated (induced shRNA expression) and untreated cell populations after 4 days of growth. Dotted lines indicate z=±3. The left panel shows shRNAs targeting MYC and luciferase as positive and

negative controls, respectively. The right panel highlights shRNAs targeting ATAD3A, BOP1 and ADRM1.

(e) Dose response curves after RNA Pol I (CX-5461) and ADRM1 (RA 190) inhibition. KPCs were treated with the indicated compounds for 48 hours and percent cell viability was measured using an MTT assay. Data are presented as mean ± SD of 6 technical replicates. IC_{50} values are shown as mean ± SD (n=3).

(f) Immunoblot of doxycycline-mediated knockdown of Atad3a in KPCs. Where indicated, cells were treated with doxycycline (1 μg/ml) for 48 h. Lysates were probed with α-Atad3a and α-Cdk2 antibodies.

(g) Analysis of cell growth in KPCs expressing either shRNA targeting luciferase or Atad3a. Where indicated, were grown in the presence of doxycycline (1 μg/ml). Cells were seeded at equal densities and either counted after 3 days (upper part) or stained with crystal violet after 4 days of growth (lower part). Data are represented as mean ± SD (n=3). The p-values were calculated using a paired two-tailed Student's t-test.

Figure 7: Functional analysis of ATAD3A.

(a) Mitochondrial localization of ATAD3A in U2OS cells. Mitochondria were immunostained with AF532 (upper part) and ATAD3A with AF647 (middle part). The overlay demonstrates co-localization of mitochondria (green) and ATAD3A (magenta) (lower part).

(b) Mitochondrial ROS levels in U2OS control cells and in cells expressing shRNAs targeting ATAD3A after doxycycline-induced MYC expression (1 μg/ml; 30 h). Data are represented as mean ± SD (n=3). p-values were calculated using a two-tailed, paired t-test.

(c) Mitochondrial ROS levels in cells transfected with control siRNA or siRNA targeting PLD6 after doxycycline-induced MYC expression. Data are represented as mean ± SD (n=3).

(d) Immunoblot showing ATAD3A knockdown by two independent shRNA constructs in U2OS cells. Lysates were probed with α-ATAD3A and α-CDK2 antibodies.

(e) MYC-dependent induction of apoptosis in U2OS control cells and cells with shRNA mediated knockdown of ATAD3A. Where indicated, MYC expression was induced by doxycycline (1 μg/ml; 36 or 48 h). AnnexinV was used to stain apoptotic cells. Data are represented as mean ± SD (n=3). The p-values were calculated using a two-tailed, paired t-test.

Figure 8: Chromatin binding and gene regulation by OmoMYC.

We propose that OmoMYC homodimers compete with MYC/MAX heterodimers for binding to DNA. Binding of MYC/MAX to promoters that are highly occupied by physiological MYC levels is stabilized by protein/protein interactions involving the MYC amino-terminus that are not outcompeted by OmoMYC. As a result, competition by OmoMYC is not uniform and is more effective on "low-affinity" promoters that are invaded by oncogenic MYC levels.

Figure 1 Jung et al.

a

Zip

HLH

C91
C91

K81
N77 N77

T63
T63

b

MYC/MAX

Zip

HLH

b

G
H906
C
E910
A
R914
G

G
H12
C
E16
A
R20
G

c

| H | L | H | Zip |

Omo RRNELKRSFFALRDQIPELENNEKAPKVVILKKATAYILSVQAETQKLISEIDLLRKQNEQLKHKLEQLRNSCA

Omo RRNELKRSFFALRDQIPELENNEKAPKVVILKKATAYILSVQAETQKLISEIDLLRKQNEQLKHKLEQLRNSCA

MYC RRNELKRSFFALRDQIPELENNEKAPKVVILKKATAYILSVQAEEQKLISEEDLLRKRREQLKHKLEQLRNSCA

MAX RRDHIKDSFHSLRDSVPSLQG-EKASRAQILDKATEYIQYMRRKNHTHQQDIDDLKRQNALLEQQVRALEKARS

- mutation (red dot)
- salt bridge (green)
- hydrophobic IA (orange)
- hydrogen bond (blue)
- disulfide bond (gray)
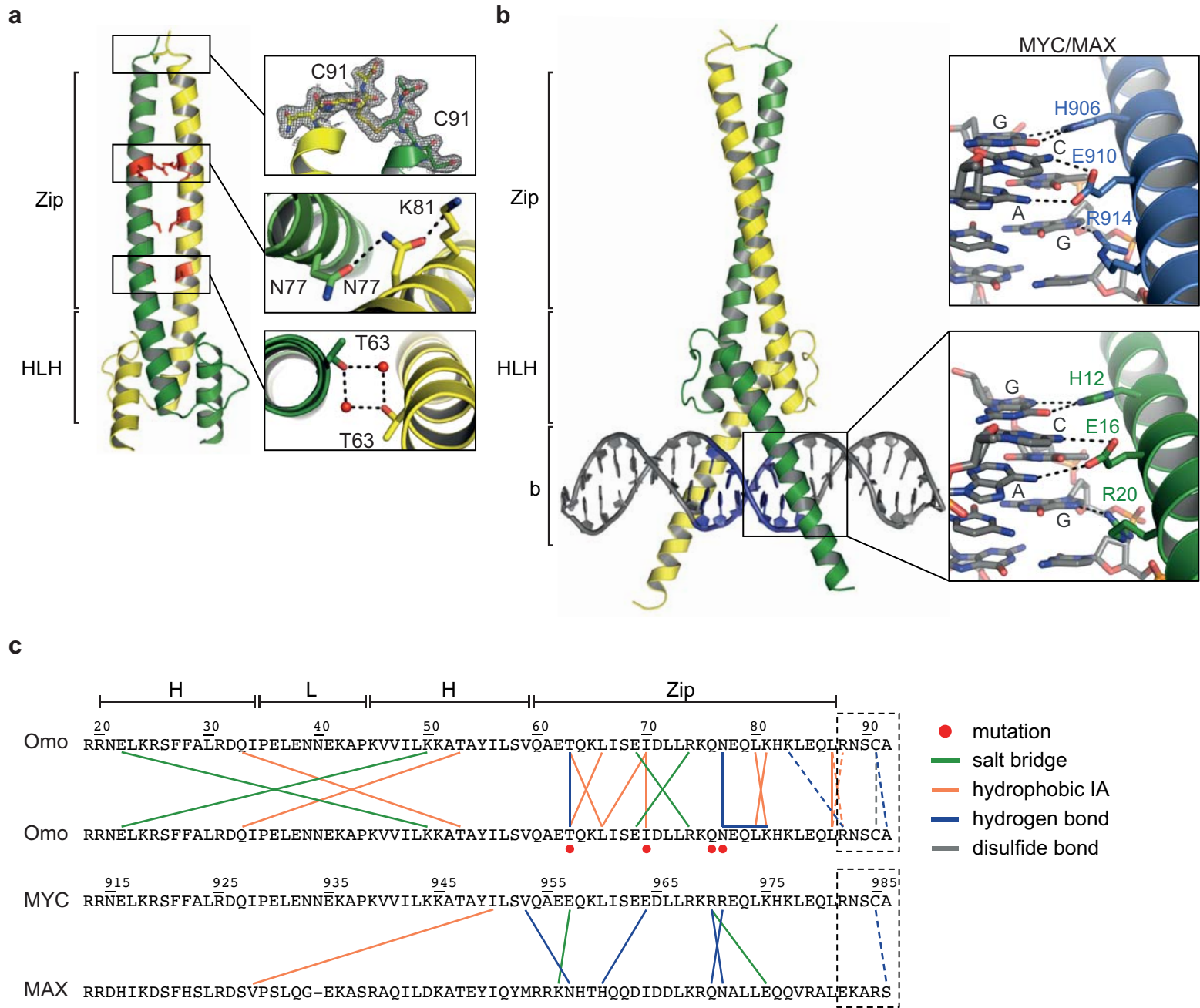
Figure 2 Jung et al.

a

b

	log Kd [M]	Kd [nM]	95 % CI
Omo + DTT	-6,408	391	-6,446 to -6,371
Omo - DTT	-6,413	386	-6,441 to -6,384
MYC/MAX	-6,314	485	-6,362 to -6,265
MYC/Omo	-6,252	560	-6,272 to -6,233
MAX	-6,213	612	-6,263 to -6,163

c

d

Figure 3 Jung et al.

a

HA-OmoMYC   −   +
DOX   −   +   −   +

α-HA
α-MYC
α-CDK2

b

5 kb   CACGTG   input

normalized tags

50
50   − DOX
50   + DOX   − OmoMYC
50   − DOX   + OmoMYC   MYC
50   + DOX
50   + DOX   − OmoMYC   HA
50   + DOX   + OmoMYC

NPM1

2 kb   CACGTG   input

normalized tags

30
30   − DOX
30   + DOX   − OmoMYC
30   − DOX   + OmoMYC   MYC
30   + DOX
30   + DOX   − OmoMYC   HA
30   + DOX   + OmoMYC

ARC

c

HA-OmoMYC   − − + + − + − − −
DOX   − + − + + + − − −

IP   input   MYC   HA   H3K4me1 H3K4me3 H3K27ac

promoter
n=10 853

intergenic
n=8 586

10 kb   0   30
               tags

d

Promoter peaks

tag density [tags/50bp]

30

15

0
           −3   0   3

Intergenic peaks

tag density [tags/50bp]

30

15

0
           −3   0   3
           distance to peak [kb]

input   +DOX −OmoMYC   −DOX −OmoMYC
IgG   +DOX +OmoMYC   −DOX +OmoMYC

e

slope=0.588
r=0.911

3

MYC recruitment [FC]
+DOX +OmoMYC / −DOX −OmoMYC

2

p=1.6x10^{-7}

1

1   2   3
MYC recruitment [FC]
+DOX −OmoMYC / −DOX −OmoMYC

Figure 4 Jung et al.

Figure 5 Jung et al.

a

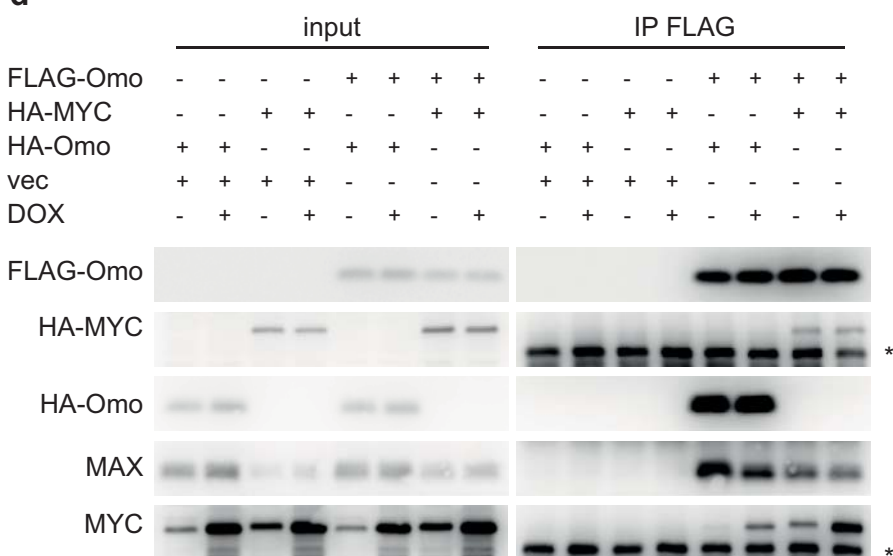|	MYC(DOX)-regulated		OmoMYC-regulated	
	NES	q-value	NES	q-value
Ben-Porath: MYC targets with E-box	1.7	6.9e-2	-1.8	4.0e-2
Dang: Regulated by MYC up	1.8	4.1e-2	-1.5	2.0e-1
Kim: MYC amplification targets down	-1.9	5.2e-3	1.8	6.8e-2
Kim: MYCN amplification targets down	-2.0	1.4e-3	2.0	6.2e-3

b

c

	OmoMYC-repressed		MYC-activated & OmoMYC-repressed		OmoMYC-activated	
	NES	p-value	NES	p-value	NES	p-value
Medulloblastoma (G4/SHH vs G3)	-1.6	1.4e-4	-1.7	4.6e-4	1.3	4.9e-2
Multiple myeloma (low MYC vs high MYC)	-2.2	<1.0e-5	-2.2	<1.0e-5	1.3	4.1e-2
Neuroblastoma (non-ampl vs NMYC-ampl)	-2.4	<1.0e-5	-2.5	<1.0e-5	1.3	7.9e-2
Colorectal carcinoma (normal mucosa vs tumor)	-2.3	<1.0e-5	-2.4	<1.0e-5	-1.2	1.6e-1
Burkitt lymphoma (median MYC expression)	-2.0	7.7e-3	-1.6	4.7e-2	-0.6	9.0e-1

d

	OmoMYC-repressed		MYC-activated & OmoMYC-repressed		OmoMYC-activated	
Eμ-MYC (control vs tumor)	-1.8	<1.0e-5	-2.1	<1.0e-5	1.0	4.8e-1
Eμ-MYC (control vs pretumor)	-1.6	<1.0e-5	-1.8	3.1e-4	-0.9	5.7e-1
Eμ-MYC (pretumour vs tumor)	-1.3	2.0e-2	-1.2	1.6e-1	1.2	1.9e-1

e

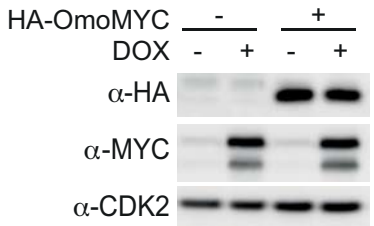|	OmoMYC-repressed		OmoMYC-activated	
	NES	p-value	NES	p-value
MEF Myc$^{-/-}$ MYCER (control vs OHT)	0.8	9.4e-1	1.2	1.9e-1
MEF Myc$^{fl/fl, CreER}$ (OHT vs control)	-0.9	6.6e-1	1.1	3.2e-1
MEF Myc$^{fl/fl, CreER}$ (OHT+serum vs control)	1.1	3.4e-1	0.9	5.8e-1

Figure 6 Jung et al.

a

vec   HA-OmoMYC
-    +   -   +   DOX

α-HA

α-Cdk2

b

cell number [x10^6]

p=0.405   p=0.007

crystal violet

-    +   -   +   DOX
vec   OmoMYC

c

MYC-acitvated genes (FDR < 0.05)

801

15 312 genes expressed → 145 → protein or pathway druggable → 27 targets

377

OmoMYC-repressed genes (FDR < 0.05)

d

+DOX / -DOX [z-score for log$_2$FC]

shRNAs - Luciferase
shRNAs - MYC

shRNAs in screen

shRNAs - ATAD3A
shRNAs - BOP1
shRNAs - ADRM1

shRNAs in screen

e

CX 5461

cell viability [%]

IC$_{50}$= 24.45 ± 2.84 nM

concentration [logM]

RA 190

cell viability [%]

IC$_{50}$= 690.3 ± 82.7 nM

concentration [logM]

g

cell number [x10^6]

p=0.129   p=0.0299   p=0.0003

crystal violet

DOX   -   +   -   +   -   +
shLuci   shAtad3a #1   shAtad3a #2

f

shLuci   shAtad3a #1   shAtad3a #2
-    +   -   +   -   +   DOX

α-Atad3a

α-Cdk2

Figure 7 Jung et al.

a

Mitochondria (AF532)

ATAD3A (AF647)

Overlay (two colour)

b

c

d

e

Figure 8 Jung et al.